Impact of Graphene Quantum Dot Edge Morphologies on Their Optical Properties

Shahriar N. Khan, Braden M. Weight, Brendan J. Gifford, Sergei Tretiak,* and Alan Bishop*

Read Online

ACCESS | Metrics & More | Article Recommendations | Supporting Information

ABSTRACT: The optoelectronic properties of functionalized graphene quantum dots (GQDs) have been explored by simulating electronic structure of three different shapes of GQDs containing exclusively zigzag or armchair edges in both pristine and functionalized forms. Absorption spectra and transition densities for the low-lying excited states are evaluated by using time-dependent density functional theory and compared for different functionalization species. The functionalization position dictates the optical properties of square GQDs, where isomers with CH_2 in the intermediate positions (excluding corner and center positions) have higher electronic transition energies and exciton delocalization than other isomers. Rhombic GQDs with all armchair edges exhibit high steric flexibility, and their complete passivation results in the largest structural deformation from planarity and strongest red-shifts. A steady red-shift in the absorption energy is observed following the order F, CH_3, Cl, and Br substitutions. This suggests that the steric effects due to large van der Waals radii overcome electronegative effects.
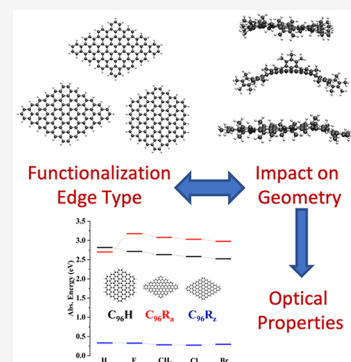
Since the first report on the synthesis and purification of carbon dots was published in 2004,[1] an exciting chapter of scientific research has commenced focused on these carbon-based nonmetallic nanomaterials with tunable optical properties. These nanomaterials exhibit bright photoluminescence, low toxicity, biocompatibility, high photostability, solubility in a wide variety of solvents, biodegradability, low cost, and scalable synthesis.[2] Active research is ongoing on both the theoretical and experimental fronts searching for next-generation nanomaterials with enhanced functionality for numerous applications such as light-emitting devices,[3−6] optoelectronic devices,[7−10] photocatalysts,[11] biomedical imaging and sensing,[12−14] functional materials,[15,16] anticounterfeiting,[17] cancer therapy,[18] and theranostics.[19]

Graphene quantum dots (GQDs) are carbon-based nanoparticles (sizes <100 nm) with a nexus of sp^2-hybridized carbon atoms.[20] Usually, a top-down approach is used to synthesize GQDs.[21−23] Different shapes of pure GQDs such as hexagonal[24] and triangular[25,26] have been synthesized and characterized. GQDs exhibit strong photoluminescence[27−29] attributed to strong quantum confinement and edge effects.[23,30] Tuning of their optical properties can be accomplished through chemical functionalization.[31−33] The effect of functionalization is dependent on the group's electron-donating and electron-withdrawing capacities. Many studies have been performed to characterize these properties.[34−36] Small finite size GQDs exhibit sizable band gaps which decrease with increasing size of the dot, as indicated by a red-shift in the emission band.[29] To tune the optical properties of pure GQDs, heteroatom doping, surface functionalization, and/or various defects have been introduced. Depending on

the nature of the defect, the electronic structure of the graphene can be modified. For instance, the existence of a free edge on the zigzag edge results in a stable triplet ground state.[37]

In this work, we have investigated the electronic and optical properties of GQDs using density functional theory (DFT), focusing on the effects of capping position (producing numerous "isomers") as well as backbone shapes and full-edge functionalization. We summarize our findings for (a) the C_{120} square GQD and its isomers, (b) the C_{96} GQD with hexagonal and rhombic shapes composed of either all-zigzag or all-armchair edge types, and (c) the complete edge passivation of the C_{96} flake with electron-donating (CH_3) or electron-withdrawing (F, Cl, Br) groups. The effect of different substituents in the electronic and optical properties is found to heavily depend on the edge type of the corresponding GQD. For different isomers of C_{120} GQDs, the position of the four CH_2 functional groups dictates the electronic (delocalization of electron) and optical (absorption energy) properties of the corresponding GQD. Also, for C_{96} GQDs, the impact of functionalization of edges where only one type of edge is present (all-armchair or all-zigzag edges) is attributed to the warping/bending of the GQDs with complete edge passivation.
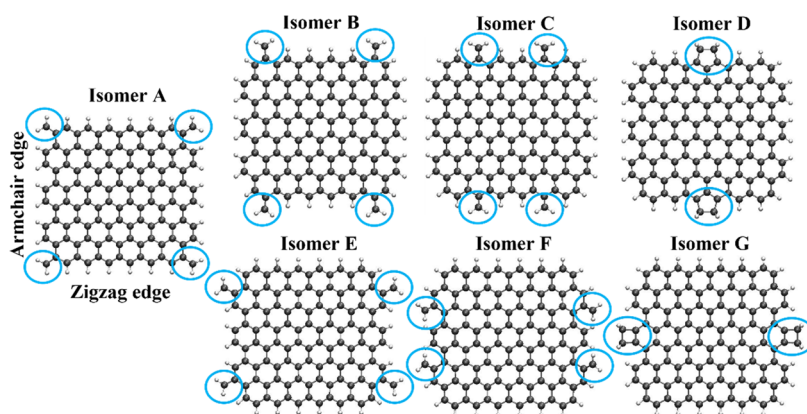
Figure 1. Atomistic models for isomers of functionalized C_{120} square GQDs.

The newly observed dependence of optical properties on the edge-type of functionalization is an important consideration of synthetic approaches of GQD-based materials targeting finely tuned homogeneous emission for light-emitted devices, photodetectors, quantum emitters, and other optoelectronic applications.[38−40]

Ground-state geometry optimization and vertical transitions in the Franck−Condon regime were computed by using DFT and time-dependent DFT (TD-DFT) using the hybrid, range-corrected CAM-B3LYP functional with a 6-31G basis set as implemented by the Gaussian 16 software package.[41] This level of theory is justified by our previous calculations on similar systems, namely, those of single-walled carbon nanotubes (SWCNTs).[42−45] The excited states were characterized by their absorption spectra produced by broadening calculated transition by a finite-width Gaussian (σ_{FWHM} = 10 meV). In addition, natural transition orbitals (NTOs)[46] and transition densities were calculated, as implemented in the Gaussian 16 and Multiwfn[47] packages, respectively.

We have studied the electronic and optical properties of square GQDs composed of 120 carbon atoms. For the model C_{120} square graphene, four CH_2 groups were placed at the four corners of the GQC and denoted as Isomer A. Other isomers of C_{120} graphene were generated by varying the positions of the four CH_2 groups. Square GQDs have two distinct types of edges denoted as zigzag and armchair. For the other isomers, the four CH_2 groups are placed on a symmetric position either on the zigzag or armchair edges. We considered a total of seven isomers: Isomers B, C, and D, where four CH_2 groups were placed along the zigzag edges, and isomers E, F, and G, where four CH_2 groups were placed along the armchair edges. Figure 1 represents all considered isomers for the C_{120} square GQD.

One additional feature for isomer D and Isomer G is that because of the proximity of the CH_2 groups, these species form nonconjugated five- and four-membered rings. As will be discussed later, these smaller rings impact the electronic and properties of these species. However, these structures are expected to have high destabilization energy due to sterics and will therefore not be very prominent species.

The optical properties can be probed in many ways. Photoluminescence is the simplest and most readily available experimental tool. To analyze optical transitions, we have performed TD-DFT (time-dependent DFT) calculations to computed the energies and oscillator strengths of the singlet electronic excitations. Figure S1 depicts the calculated absorption spectra of each of the isomers. The lowest optically

allowed (bright) state is an important characteristic for applications requiring single-photon emission and sensing. For isomer A, the first bright transition is the seventh singlet excited state, S_7, at 0.74 eV. Then for isomers B and C, the absorption energies of the first bright transition increases to 1.62 eV (S_2) and 1.76 eV (S_1), respectively. In comparison, isomers E and F have absorption energies at 0.87 eV (S_8) and 1.71 eV (S_1), respectively. Very similar spectra are found for isomers D and G with the first bright transition at 0.68 eV (S_1) and 0.75 eV (S_1), respectively. This is intuitively clear from their shared nonconjugated four- and five-membered rings, which will have a localizing effect on the low-lying excitons. Clearly, the optical properties are extremely sensitive to the placement of the four CH_2 groups, suggesting a simple approach to tuning these GQDs' properties. Scheme 1 depicts

Scheme 1. Comparison of the Energies of the Lowest Energy Transition (LET) and the First Bright Transition (FBT) for Each Isomer
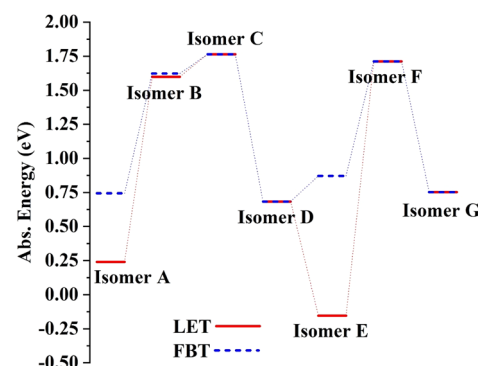
the comparison of the lowest energy transition (LET, S_1 state) for the isomers along with the comparison of the first bright transition (FBT) energies. The absorption energy of the isomers depends on the position of the capping units (CH_2). For example, CH_2 placed at the corner/center leads to lower absorption energies than the isomer C and F with capping units placed in between.

To characterize the origin of the observed spectral shifts, natural transition orbitals (NTOs)[46] and transition densities (TDs) of the relevant ground-to-excited transitions are studied. Figure S2 depicts the highest occupied transition orbitals (HOTO, characterizing a hole state) and the lowest unoccupied transition orbitals (LUTO, characterizing an

election state) for the first excited state (S_1) and for the first bright transition along with the TDs of the corresponding bright transitions.

The TDs of the first bright transitions are heavily dependent on the position of the capping units (CH_2). The associated higher absorption energies of isomers B, C, and D are corroborated with the delocalization of the TDs throughout the GQD backbone (compare Figures S1 and S2). Isomers D and G, as mentioned earlier, share similar absorption spectra (Figure S1), which is readily explained by comparing their real-space surfaces, which show very similar excitonic localization in both NTOs and TDs (Figure 2 and Figure S2).
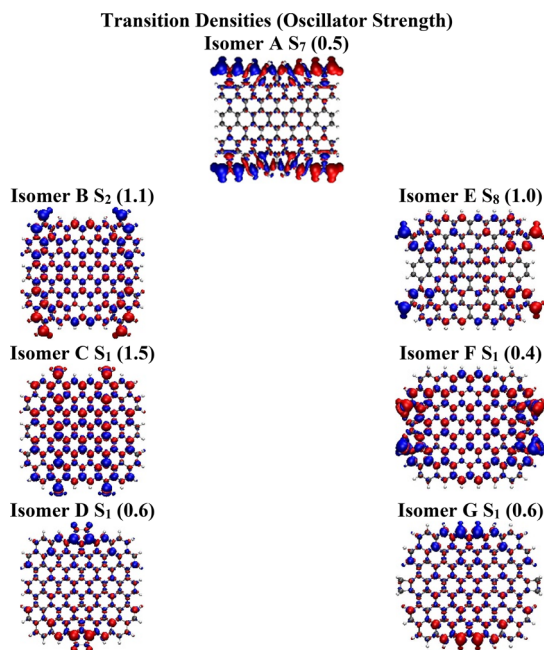
Transition Densities (Oscillator Strength)
Isomer A S_7 (0.5)

Isomer B S_2 (1.1)   **Isomer E S_8 (1.0)**

Isomer C S_1 (1.5)   **Isomer F S_1 (0.4)**

Isomer D S_1 (0.6)   **Isomer G S_1 (0.6)**

Figure 2. Transition densities for the first bright transitions of each of the isomers. The oscillator strengths are given in parentheses.

Summarizing, the electronic and optical properties of square graphene are dramatically impacted by the nature of the edge and the position of the substituents. In the next subsection we investigate graphene with only zigzag or armchair edges. For this, we examine the C_{96} graphene with hexagonal and rhombic shapes as well as with full-edge passivation with CH_3, F, Br, and Cl.

Three different shapes of C_{96} GQDs are possible, namely, hexagonal ($C_{96}H$), rhombic with all-zigzag edges ($C_{96}R_z$), and rhombic with all-armchair edges ($C_{96}R_a$). Figure 3 illustrates the atomistic models for these GQD shapes. To study the change of optical properties due to the change of the shapes of the GQDs, the absorption spectra of these species were calculated along with the spectra for the substitution of the passivating H atoms with electron donating CH_3 groups. For the $C_{96}H$ species, the transition energy of the optically dark S_1 state is 2.12 eV. States S_3 and S_4 are degenerate and are responsible for the first bright transition at 2.82 eV. For the same species with every H substituted with CH_3, the degeneracy is slightly lifted due to the deformation of the carbon backbone (as the pristine sheet is planar) and results in a red-shift of the absorption spectra by $\Delta E = E_{3,4}^H - E_{3,4}^{CH_3} = 186$ meV.
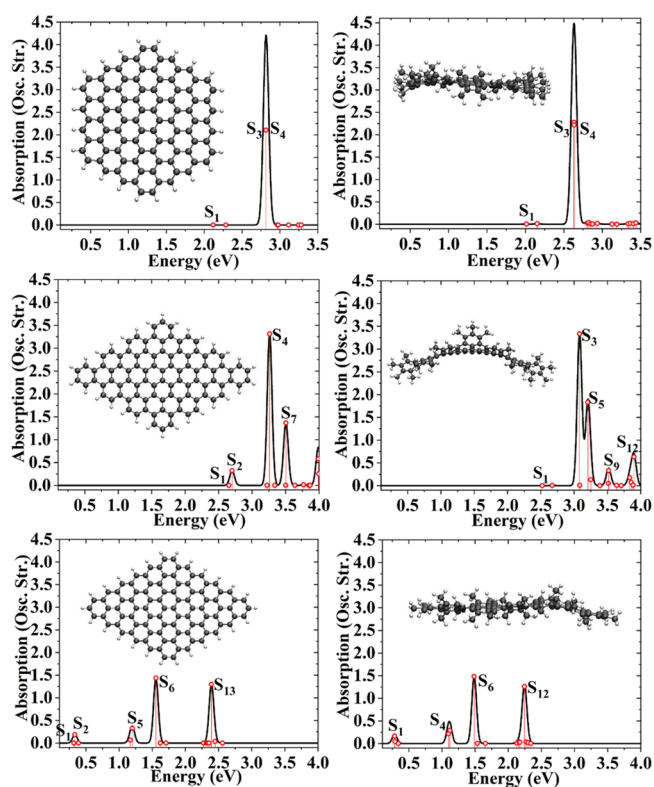

Figure 3. Comparison of absorption spectra for $C_{96}H$, $C_{96}R_a$, and $C_{96}R_z$ (left column). Change of absorption spectra of these species for CH_3 substitution induced by a break in planarity (right column).

Although the stoichiometry and size of the $C_{96}H$ remain similar to the $C_{96}R_a$, substantial differences in the spectra are observed. $C_{96}R_a$ has the first excited state S_1 at 2.65 eV, which is optically dark. The brightest optical transition is S_4 located at 3.26 eV. The structural deformation and the red-shift of the spectra for the CH_3-substituted species ($\Delta E = E_3^H - E_3^{CH_3} = 180$ meV) of nearly the same size as seen in $C_{96}H$ is present, suggesting that the red-shifts from deformation are similar for both geometries. In contrast with $C_{96}H$ and $C_{96}R_a$, the species $C_{96}R_z$ has a low-lying S_1 state at 0.32 eV. The brightest optical transition is S_6 at 1.56 eV. The CH_3 substitution deformed the pristine structure, but the deformation is not as large as for $C_{96}R_a$, which is attributed to the rigidity of the zigzag edges of $C_{96}R_z$ (see Figure 3).

To assess the change of electronic and optical properties stemming from either steric effects (CH_3 passivation) or electron-withdrawing effects, edge functionalization of all C_{96} GQD species with halogens (F, Cl, and Br) was performed. The $C_{96}R_a$ is found to be the most deformed from planarity due to larger flexibility of the armchair edge compared to $C_{96}H$ and $C_{96}R_z$ species. As the size of the substituent increases (from F to Br), the deformation becomes more prominent, leading to a mostly steric-based modification of the structure (see Figure 4). It is also notable that the deformation in $C_{96}R_a$ results in a drastically deformed "saddle" shape due to the close proximity of the passivating H groups on the edges, while the other two species show less dramatic warping.

For the $C_{96}H$ species, F, Cl, and Br functionalization at every edge site systematically red-shifts the S_1 state with transition energies 2.04, 1.98, and 1.96 eV, respectively, with a net change of 87 meV. Additionally, the gradual red-shift is present for the first bright transition (degenerate S_3 and S_4) with transition
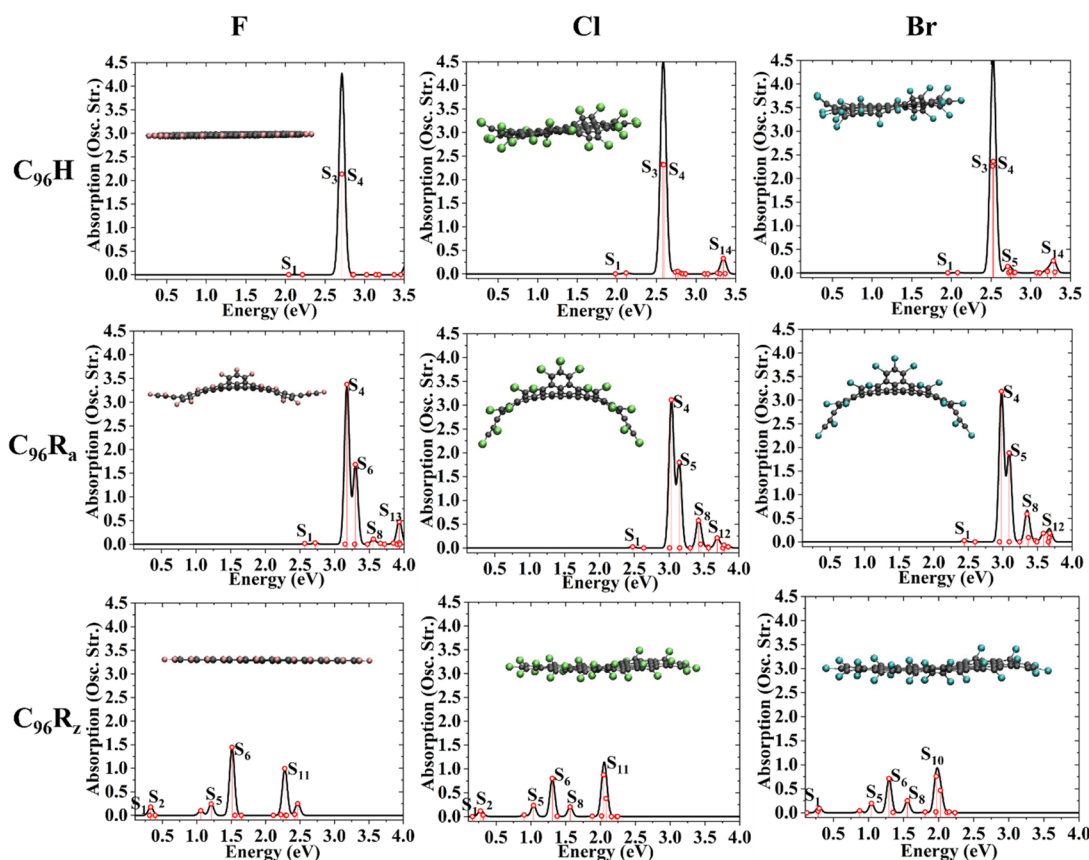
Figure 4. Comparison of the absorption spectra for completely passivated $C_{96}H$, $C_{96}R_a$, and $C_{96}R_z$ species with F, Cl, and Br presented in the first, second, and third columns, respectively.

energies of 2.71, 2.32, and 2.52 eV for substituents F, Cl, and Br, respectively, with a marked increase in net change of 193 meV, suggesting that the bright state is largely determined by the geometric deformation. Following the trend of the pristine species, functionalized $C_{96}R_a$ has a higher absorption energy, and S_1 for F, Cl, and Br is at 2.57, 2.49, and 2.44 eV, respectively. The first bright optical transition corresponds to S_4, and for F, Cl, and Br the associated energies are 3.38, 3.11, and 2.98 eV, respectively. Again, $C_{96}R_z$ with F, Cl, and Br functionalization follows the patterns of $C_{96}R_z$ pristine species with a low absorption energy for S_1 (0.31, 0.16, and 0.12 eV, respectively), while the brightest transitions of these species correspond to S_6 with the energy 1.51, 1.31, and 1.29 eV, respectively. The NTOs and TDs of the first bright transitions are reported in Figures S3−S5 for the pristine and completely passivated species. The lower absorptions energies of the $C_{96}R_z$ species can be understood by inspecting the electronic structure of S_1. These are fairly localized, whereas for $C_{96}H$ and $C_{96}R_a$ species the S_1 electronic state is delocalized throughout the GQDs.

Additionally, a comparison of the first bright transition for the edge functionalized species is summarized in Scheme 2 where electron-withdrawing halogens and electron-donating CH_3 are directly compared. For the pristine species, $C_{96}H$ has a higher absorption energy than $C_{96}R_a$ and $C_{96}R_z$, but with complete passivation with any functionalizing species $C_{96}R_a$ possesses higher absorption energy. The substituent groups produced a systematic red-shift in the order of F, CH_3, Cl, and Br. Considering the van der Waals radii of F, C, Cl, and Br

Scheme 2. Schematic of the Transition Energies of the Lowest-Energy and Bright Transitions for the Pristine and Fully Edge-Functionalized C_{96} GQDs with CH_3, F, Cl, and Br (Columns) for Each Geometry of C_{96} GQDs (Colors) (Dotted Lines Are Guides for the Eye)
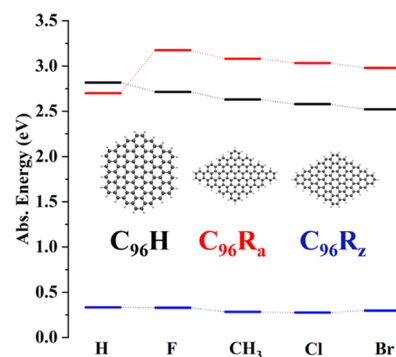
(1.47, 1.70, 1.75, and 1.85 Å, respectively), the ordering suggests a dominance of steric effects over polarization.

In summary, using density functional theory, we have studied the electronic and optical properties of C_{120} square graphene flakes. These isomers reveal that the position of the CH_2 units greatly influences the optical properties. In addition, functionalization of the zigzag edge and the armchair edge shows unique electronic properties. The position of the CH_2 units dictates the nature of the electron delocalization: the corner position and the positions at the center of either edge result in exciton edge-localization, whereas for other cases, the exciton is delocalized throughout the graphene backbone. A

higher degree of delocalization directly results in higher-energy transitions.

We also compare the optical properties of different shapes of GQDs of similar stoichiometry. C_{96} hexagonal and C_{96} rhombic shapes are studied, including two variants of the rhombic shape: all-zigzag edge ($C_{96}R_z$) and all-armchair edge ($C_{96}R_a$). $C_{96}R_a$ species have the highest-energy absorption for the bright transition at 3.26 eV. From the pristine structure, substitution of all H with CH_3 results in a distortion of the planarity of the graphene flakes accompanied by a slight red-shift on the absorption spectra. The deformation of the pristine flakes is even greater for the substitution of all H with halogens (F, Cl, and Br). The species with all armchair edges ($C_{96}R_a$) are the most deformed ones due to the additional flexibility of the edges. Also, upon comparison of the absorption spectra for the halogens, when going from F to Br, the bright transitions are red-shifted by 196 meV. Finally, a comparison of the effect of electron-donating and electron-withdrawing groups on the C_{96} graphene reveals that the type of the edge and steric effects dominate the optical properties.

Altogether, our computational study demonstrates an extreme sensitivity of the electronic structure of GQD to the shape and to the edge functionalization. This suggests that nanomaterials with nonidentical GQD species will display highly inhomogeneous electronic properties. This is in distinct contrast, for example, to semiconductor nanocrystals, where an ensemble of similar dots possesses rather similar electronic features.[45] Synthetic routes to producing molecularly identical GQDs are critical[46] and can make use of the vast tunability of electronic properties of GQDs subject to only minor structural modifications. Detailed computational results such as presented in this contribution identify trends and determine structure—electronic property relationships across the vast space of possible GQD systems. This can help to guide the ongoing experimental studies of optoelectronic properties of GQDs.[48−51]

ASSOCIATED CONTENT

Supporting Information

The Supporting Information is available free of charge at https://pubs.acs.org/doi/10.1021/acs.jpclett.2c01036.

> Absorption spectra, natural transition orbitals, and transition density dependence of functionalization position, isomer, and functionalization species (PDF)

AUTHOR INFORMATION

Corresponding Authors

Sergei Tretiak − *Theoretical Division, Center for Integrated Nanotechnologies (CINT), Los Alamos National Laboratory, Los Alamos, New Mexico 87545, United States;* orcid.org/0000-0001-5547-3647; Email: serg@lanl.gov

Alan Bishop − *Los Alamos National Laboratory, Los Alamos, New Mexico 87545, United States;* Email: arb@lanl.gov

Authors

Shahriar N. Khan − *Department of Chemistry and Biochemistry, Auburn University, Auburn, Alabama 36849-5312, United States; Theoretical Division, Center for Integrated Nanotechnologies (CINT), Los Alamos National Laboratory, Los Alamos, New Mexico 87545, United States;* orcid.org/0000-0002-8913-8430

Braden M. Weight − *Theoretical Division, Center for Integrated Nanotechnologies (CINT), Los Alamos National Laboratory, Los Alamos, New Mexico 87545, United States; Department of Physics, University of Rochester, Rochester, New York 14627, United States;* orcid.org/0000-0002-2441-3569

Brendan J. Gifford − *Theoretical Division, Center for Integrated Nanotechnologies (CINT), Los Alamos National Laboratory, Los Alamos, New Mexico 87545, United States;* orcid.org/0000-0002-4116-711X

Complete contact information is available at:
https://pubs.acs.org/10.1021/acs.jpclett.2c01036

Notes

The authors declare no competing financial interest.

REFERENCES

(1) Xu, X.; Ray, R.; Gu, Y.; Ploehn, H. J.; Gearheart, L.; Raker, K.; Scrivens, W. A. Electrophoretic Analysis and Purification of Fluorescent Single-Walled Carbon Nanotube Fragments. *J. Am. Chem. Soc.* 2004, 126, 12736−12737.

(2) Langer, M.; Paloncýová, M.; Medved', M.; Pykal, M.; Nachtigallová, D.; Shi, B.; Aquino, A. J. A.; Lischka, H.; Otyepka, M. Progress and challenges in understanding of photoluminescence properties of carbon dots based on theoretical computations. *Appl. Mater. Today* 2021, 22, 100924.

(3) Mei, S.; Liu, X.; Zhang, W.; Liu, R.; Zheng, L.; Guo, R.; Tian, P. High-Bandwidth White-Light System Combining a Micro-LED with Perovskite Quantum Dots for Visible Light Communication. *ACS Appl. Mater. Interfaces* 2018, 10, 5641−5648.

(4) Zhou, Z.; Tian, P.; Liu, X.; Mei, S.; Zhou, D.; Li, D.; Jing, P.; Zhang, W.; Guo, R.; Qu, S.; Rogach, A. L. Hydrogen Peroxide-Treated Carbon Dot Phosphor with a Bathochromic-Shifted, Aggregation-Enhanced Emission for Light-Emitting Devices and Visible Light Communication. *Adv. Sci.* 2018, 5, 1800369.

(5) Yuan, F.; Wang, Z.; Li, X.; Li, Y.; Tan, Z. A.; Fan, L.; Yang, S. Bright Multicolor Bandgap Fluorescent Carbon Quantum Dots for Electroluminescent Light-Emitting Diodes. *Adv. Mater.* 2017, 29, 1604436.

(6) Wang, Z.; Yuan, F.; Li, X.; Li, Y.; Zhong, H.; Fan, L.; Yang, S. 53% Efficient Red Emissive Carbon Quantum Dots for High Color Rendering and Stable Warm White-Light-Emitting Diodes. *Adv. Mater.* 2017, 29, 1702910.

(7) Semeniuk, M.; Yi, Z.; Poursorkhabi, V.; Tjong, J.; Jaffer, S.; Lu, Z.-H.; Sain, M. Future Perspectives and Review on Organic Carbon Dots in Electronic Applications. *ACS Nano* 2019, 13, 6224−6255.

(8) Tetsuka, H.; Nagoya, A.; Fukusumi, T.; Matsui, T. Molecularly Designed, Nitrogen-Functionalized Graphene Quantum Dots for Optoelectronic Devices. *Ad. Mater.* 2016, 28, 4632−4638.

(9) Arcudi, F.; Strauss, V.; Ðorđević, L.; Cadranel, A.; Guldi, D. M.; Prato, M. Porphyrin Antennas on Carbon Nanodots: Excited State

Energy and Electron Transduction. *Agnew. Chem., Int. Ed.* **2017**, *56*, 12097−12101.

(10) Yuan, T.; Meng, T.; He, P.; Shi, Y.; Li, Y.; Li, X.; Fan, L.; Yang, S. Carbon quantum dots: an emerging material for optoelectronic applications. *J. Mater. Chem. C* **2019**, *7*, 6820−6835.

(11) Liu, J.; Liu, Y.; Liu, N.; Han, Y.; Zhang, X.; Huang, H.; Lifshitz, Y.; Lee, S.-T.; Zhong, J.; Kang, Z. Metal-free efficient photocatalyst for stable visible water splitting via a two-electron pathway. *Sci.* **2015**, *347*, 970−974.

(12) Misra, S. K.; Srivastava, I.; Tripathi, I.; Daza, E.; Ostadhossein, F.; Pan, D. Macromolecularly "Caged" Carbon Nanoparticles for Intracellular Trafficking via Switchable Photoluminescence. *J. Am. Chem. Soc.* **2017**, *139*, 1746−1749.

(13) Rizzo, C.; Arcudi, F.; Đorđević, L.; Dintcheva, N. T.; Noto, R.; D'Anna, F.; Prato, M. Nitrogen-Doped Carbon Nanodots-Ionogels: Preparation, Characterization, and Radical Scavenging Activity. *ACS Nano* **2018**, *12*, 1296−1305.

(14) Xu, X.; Zhang, K.; Zhao, L.; Li, C.; Bu, W.; Shen, Y.; Gu, Z.; Chang, B.; Zheng, C.; Lin, C.; Sun, H.; Yang, B. Aspirin-Based Carbon Dots, a Good Biocompatibility of Material Applied for Bioimaging and Anti-Inflammation. *ACS Appl. Mater. Interfaces* **2016**, *8*, 32706−32716.

(15) Zhang, M.; Hu, L.; Wang, H.; Song, Y.; Liu, Y.; Li, H.; Shao, M.; Huang, H.; Kang, Z. One-step hydrothermal synthesis of chiral carbon dots and their effects on mung bean plant growth. *Nanoscale* **2018**, *10*, 12734−12742.

(16) Shan, X.; Chai, L.; Ma, J.; Qian, Z.; Chen, J.; Feng, H. B-doped carbon quantum dots as a sensitive fluorescence probe for hydrogen peroxide and glucose detection. *Analyst* **2014**, *139*, 2322−2325.

(17) Kalytchuk, S.; Wang, Y.; Poláková, K.; Zbořil, R. Carbon Dot Fluorescence-Lifetime-Encoded Anti-Counterfeiting. *ACS Appl. Mater. Interfaces* **2018**, *10*, 29902−29908.

(18) Kim, T. H.; Sirdaarta, J. P.; Zhang, Q.; Eftekhari, E.; St. John, J.; Kennedy, D.; Cock, I. E.; Li, Q. Selective toxicity of hydroxyl-rich carbon nanodots for cancer research. *Nano Res.* **2018**, *11*, 2204−2216.

(19) Li, S.; Su, W.; Wu, H.; Yuan, T.; Yuan, C.; Liu, J.; Deng, G.; Gao, X.; Chen, Z.; Bao, Y.; Yuan, F.; Zhou, S.; Tan, H.; Li, Y.; Li, X.; Fan, L.; Zhu, J.; Chen, A. T.; Liu, F.; Zhou, Y.; Li, M.; Zhai, X.; Zhou, J. Targeted tumour theranostics in mice via carbon quantum dots structurally mimicking large amino acids. *Nat. Biomed. Eng.* **2020**, *4*, 704−716.

(20) Chung, S.; Revia, R. A.; Zhang, M. Graphene Quantum Dots and Their Applications in Bioimaging, Biosensing, and Therapy. *Adv. Mater.* **2021**, *33*, 1904362.

(21) Lu, J.; Yang, J.-x.; Wang, J.; Lim, A.; Wang, S.; Loh, K. P. One-Pot Synthesis of Fluorescent Carbon Nanoribbons, Nanoparticles, and Graphene by the Exfoliation of Graphite in Ionic Liquids. *ACS Nano* **2009**, *3*, 2367−2375.

(22) Hola, K.; Zhang, Y.; Wang, Y.; Giannelis, E. P.; Zboril, R.; Rogach, A. L. Carbon dots—Emerging light emitters for bioimaging, cancer therapy and optoelectronics. *Nano Today* **2014**, *9*, 590−603.

(23) Jin, S. H.; Kim, D. H.; Jun, G. H.; Hong, S. H.; Jeon, S. Tuning the Photoluminescence of Graphene Quantum Dots through the Charge Transfer Effect of Functional Groups. *ACS Nano* **2013**, *7*, 1239−1245.

(24) Lee, S. H.; Kim, D. Y.; Lee, J.; Lee, S. B.; Han, H.; Kim, Y. Y.; Mun, S. C.; Im, S. H.; Kim, T.-H.; Park, O. O. Synthesis of Single-Crystalline Hexagonal Graphene Quantum Dots from Solution Chemistry. *Nano Lett.* **2019**, *19*, 5437−5442.

(25) Yuan, F.; Yuan, T.; Sui, L.; Wang, Z.; Xi, Z.; Li, Y.; Li, X.; Fan, L.; Tan, Z. A.; Chen, A.; Jin, M.; Yang, S. Engineering triangular carbon quantum dots with unprecedented narrow bandwidth emission for multicolored LEDs. *Nat. Commun.* **2018**, *9*, 2249.

(26) Yuan, F.; He, P.; Xi, Z.; Li, X.; Li, Y.; Zhong, H.; Fan, L.; Yang, S. Highly efficient and stable white LEDs based on pure red narrow bandwidth emission triangular carbon quantum dots for wide-color gamut backlight displays. *Nano Res.* **2019**, *12*, 1669−1674.

(27) Li, M.; Wu, W.; Ren, W.; Cheng, H.-M.; Tang, N.; Zhong, W.; Du, Y. Synthesis and upconversion luminescence of N-doped graphene quantum dots. *Appl. Phys. Lett.* **2012**, *101*, 103107.

(28) Liu, R.; Wu, D.; Feng, X.; Müllen, K. Bottom-Up Fabrication of Photoluminescent Graphene Quantum Dots with Uniform Morphology. *J. Am. Chem. Soc.* **2011**, *133*, 15221−15223.

(29) Kim, S.; Hwang, S. W.; Kim, M.-K.; Shin, D. Y.; Shin, D. H.; Kim, C. O.; Yang, S. B.; Park, J. H.; Hwang, E.; Choi, S.-H.; Ko, G.; Sim, S.; Sone, C.; Choi, H. J.; Bae, S.; Hong, B. H. Anomalous Behaviors of Visible Luminescence from Graphene Quantum Dots: Interplay between Size and Shape. *ACS Nano* **2012**, *6*, 8203−8208.

(30) Sun, H.; Wu, L.; Wei, W.; Qu, X. Recent advances in graphene quantum dots for sensing. *Mater. Today* **2013**, *16*, 433−442.

(31) Park, H.; Hyun Noh, S.; Hye Lee, J.; Jun Lee, W.; Yun Jaung, J.; Geol Lee, S.; Hee Han, T. Large Scale Synthesis and Light Emitting Fibers of Tailor-Made Graphene Quantum Dots. *Sci. Rep.* **2015**, *5*, 14163.

(32) Wang, Y.; Kong, W.; Wang, L.; Zhang, J. Z.; Li, Y.; Liu, X.; Li, Y. Optimizing oxygen functional groups in graphene quantum dots for improved antioxidant mechanism. *Phys. Chem. Chem. Phys.* **2019**, *21*, 1336−1343.

(33) Jabed, M. A.; Zhao, J.; Kilin, D.; Yu, T. Understanding of Light Absorption Properties of the N-Doped Graphene Oxide Quantum Dot with TD-DFT. *J. Phys. Chem. C* **2021**, *125*, 14979−14990.

(34) Kuo, W.-S.; Chang, C.-Y.; Huang, K.-S.; Liu, J.-C.; Shao, Y.-T.; Yang, C.-H.; Wu, P.-C. Amino-Functionalized Nitrogen-Doped Graphene-Quantum-Dot-Based Nanomaterials with Nitrogen and Amino-Functionalized Group Content Dependence for Highly Efficient Two-Photon Bioimaging. *Int. J. Mol. Sci.* **2020**, *21*, 2939.

(35) Sweetman, M. J.; Hickey, S. M.; Brooks, D. A.; Hayball, J. D.; Plush, S. E. A Practical Guide to Prepare and Synthetically Modify Graphene Quantum Dots. *Adv. Funct. Mater.* **2019**, *29*, 1808740.

(36) Zhu, S.; Shao, J.; Song, Y.; Zhao, X.; Du, J.; Wang, L.; Wang, H.; Zhang, K.; Zhang, J.; Yang, B. Investigating the surface state of graphene quantum dots. *Nanoscale* **2015**, *7*, 7927−7933.

(37) Pan, D.; Zhang, J.; Li, Z.; Wu, M. Hydrothermal Route for Cutting Graphene Sheets into Blue-Luminescent Graphene Quantum Dots. *Adv. Mater.* **2010**, *22*, 734−738.

(38) Zhao, S.; Lavie, J.; Rondin, L.; Orcin-Chaix, L.; Diederichs, C.; Roussignol, P.; Chassagneux, Y.; Voisin, C.; Mullen, K.; Narita, A.; Campidelli, S.; Lauret, J. Single Photon Emission from Graphene Quantum Dots at Room Temperature. *Nat. Commun.* **2018**, *9*, 3470.

(39) Chen, Y.; Lu, D.; Wang, G.; Huangfu, J.; Wu, Q.; Wang, X.; Liu, L.; Ye, D.; Yan, B.; Han, J. Highly Efficient Orange Emissive Graphene Quantum Dots Prepared by Acid-Free Method for White LEDs. *ACS Sustain. Chem. Eng.* **2020**, *8*, 6657−6666.

(40) Liu, Z.; Qiu, H.; Fu, S.; Wang, C.; Yao, X.; Dixon, A. G.; Campidelli, S.; Pavlica, E.; et al. Solution-processed graphene−nanographene van der Waals heterostructures for photodetectors with efficient and ultralong charge separation. *J. Am. Chem. Soc.* **2021**, *143*, 17109.

(41) Frisch, M. J.; Trucks, G. W.; Schlegel, H. B.; Scuseria, G. E.; Robb, M. A.; Cheeseman, J. R.; Scalmani, G.; Barone, V.; Petersson, G. A.; Nakatsuji, H.; Li, X.; Caricato, M.; Marenich, A. V.; Bloino, J.; Janesko, B. G.; Gomperts, R.; Mennucci, B.; Hratchian, H. P.; Ortiz, J. V.; Izmaylov, A. F.; Sonnenberg, J. L.; Williams; Ding, F.; Lipparini, F.; Egidi, F.; Goings, J.; Peng, B.; Petrone, A.; Henderson, T.; Ranasinghe, D.; Zakrzewski, V. G.; Gao, J.; Rega, N.; Zheng, G.; Liang, W.; Hada, M.; Ehara, M.; Toyota, K.; Fukuda, R.; Hasegawa, J.; Ishida, M.; Nakajima, T.; Honda, Y.; Kitao, O.; Nakai, H.; Vreven, T.; Throssell, K.; Montgomery, Jr., J. A.; Peralta, J. E.; Ogliaro, F.; Bearpark, M. J.; Heyd, J. J.; Brothers, E. N.; Kudin, K. N.; Staroverov, V. N.; Keith, T. A.; Kobayashi, R.; Normand, J.; Raghavachari, K.; Rendell, A. P.; Burant, J. C.; Iyengar, S. S.; Tomasi, J.; Cossi, M.; Millam, J. M.; Klene, M.; Adamo, C.; Cammi, R.; Ochterski, J. W.; Martin, R. L.; Morokuma, K.; Farkas, O.; Foresman, J. B.; Fox, D. J. *Gaussian 16*, Rev. C.01; Gaussian, Inc.: Wallingford, CT, 2016.

(42) Kim, Y.; Goupalov, S. V.; Weight, B. M.; Gifford, B. J.; He, X.; Saha, A.; Kim, M.; Ao, G.; Wang, Y.; Zheng, M.; Tretiak, S.; Doorn, S.

K.; Htoon, H. Hidden Fine Structure of Quantum Defects Revealed by Single Carbon Nanotube Magneto-Photoluminescence. *ACS Nano* **2020**, *14*, 3451−3460.

(43) Weight, B. M.; Sifain, A. E.; Gifford, B. J.; Kilin, D.; Kilina, S.; Tretiak, S. Coupling between Emissive Defects on Carbon Nanotubes: Modeling Insights. *J. Phys. Chem. Lett.* **2021**, *12*, 7846−7853.

(44) Weight, B. M.; Gifford, B. J.; Tretiak, S.; Kilina, S. Interplay between Electrostatic Properties of Molecular Adducts and Their Positions at Carbon Nanotubes. *J. Phys. Chem. C* **2021**, *125*, 4785−4793.

(45) Sheely, A.; Gifford, B.; Tretiak, S.; Bishop, A. Tunable Optical Features of Graphene Quantum Dots from Edge Functionalization. *J. Phys. Chem. C* **2021**, *125*, 9244−9252.

(46) Martin, R. L. Natural transition orbitals. *J. Chem. Phys.* **2003**, *118*, 4775−4777.

(47) Lu, T.; Chen, F. Multiwfn: A multifunctional wavefunction analyzer. *J. Comput. Chem.* **2012**, *33*, 580−592.

(48) Garcia de Arquer, F. P.; Talapin, D. V.; Klimov, V. I.; Arakawa, Y.; Bayer, M.; Sargent, E. H. Semiconductor quantum dots: Technological progress and future challenges. *Science* **2021**, *373*, 8541.

(49) Xiao, D.; Qi, H.; Teng, Y.; Pierre, D.; Kutoka, P. T.; Liu, D. Advances and Challenges of Fluorescent Nanomaterials for Synthesis and Biomedical Applications. *Nanoscale Res. Lett.* **2021**, *16*, 167.

(50) Liu, T.; Carles, B.; Elias, C.; Tonnelé, C.; Medina-Lopez, D.; Narita, A.; et al. Vibronic fingerprints in the luminescence of graphene quantum dots at cryogenic temperature. *J. Chem. Phys.* **2022**, *156*, 104302.

(51) Liu, T.; Tonnelé, C.; Zhao, S.; Rondin, L.; Elias, C.; Medina-Lopez, D.; Okuno, H.; et al. Vibronic effect and influence of aggregation on the photophysics of graphene quantum dots. *Nanoscale* **2022**, *14*, 3826.